A Dual-Radar Noise Compensation System for UAV-Born Cardiopulmonary Vital Signs Detection

Khaldoon M. Ishmael, *Member, IEEE*, Shekh M. M. Islam, *Senior Member, IEEE*, Mohammad Shadman Ishrak, *Graduate Student Member, IEEE*, Jannatun Noor Sameera, *Graduate Student Member, IEEE*, Richard C. Ordoñez, *Member, IEEE*, Victor M. Lubecke, *Fellow, IEEE*, and Olga Borić-Lubecke, *Fellow, IEEE*

***Abstract*—Uncrewed aerial vehicles (UAVs) equipped with Doppler radar for remote life sensing have the potential to offer an effective solution for search and rescue applications. Interference introduced by the moving UAV platform can, however, obscure human vital signs. A dual 24-GHz radar noise compensation (DRNC) system is proposed with two motion compensation methods: adaptive noise cancellation (ANC) and net signal interference cancellation (NIC). Arctangent-demodulated platform motion reference signals are used to enable accurate recovery of respiration displacement. The proposed methods have been validated with a robotic mover and a human subject, showing a motion frequency error of less than 1% and a respiration displacement error of less than 10%. The respiration displacement error was a fraction of 1 mm, even in the presence of a platform motion that exceeded 100 mm. To the best of the authors' knowledge, this is the first use of arctangent demodulation for ANC motion reference and the first UAV in-flight measurement of human respiration displacement.**

***Index Terms*—Airborne biosensors, doppler radar, noise cancellation, noise reduction, radar detection, signal processing, uncrewed aerial vehicles (UAVs).**

I. Introduction

ADVANCEMENTS in uncrewed aerial vehicles (UAVs) technology have made drones commonplace tools for challenging surveillance operations ranging from agriculture to security operations [1]. Although most of these operations are based on a camera for surveillance, UAV-born radar motion sensors promise to significantly extend the functionality of such systems to detect critical measures where visual imagery is unsuitable due to obstruction or privacy issues. For example, in applications such as postdisaster assessment, a UAV equipped with a radar motion detection system can be used to assess the cardiopulmonary vital signs of an otherwise motionless victim, even when the view of the subject is obscured by heavy clothing, smoke, or fog [2].

UAVs are mobile platforms that introduce their own motion, which, however, appears in radar measurements and obscures the motion signal of interest [3]. Basic UAV stabilization methods are generally not adequate for robust vital signs detection, which can accurately capture variations in torso displacement during uncontrolled flight. Previous research has demonstrated that a UAV flight control system can use motion sensed by inertial mass units (IMUs), ultrasonic range sensors, radio direction of arrival (DOA), and received signal strength indicators (RSSIs) to provide flight control feedback to produce a stable platform suitable for sensing in some situations [4]. Other systems have demonstrated motion compensation in front of a vertical subject with complex multimodal sensing, including the use of IMUs, lidar sensors, and mechanically rotating or MIMO radars [5], [6]. Although such methods provide convincing demonstrations for various motion compensation mechanisms, they depend on a fairly complex combination of signals and sensors. Practical situations depend on the lowest cost/complexity, which can provide satisfactory motion compensation while preserving an accurate respiratory displacement waveform.

Attempts to sense human cardiopulmonary vital signs from a moving platform using radar alone have been limited to postprocessed synthetic aperture radar (SAR) images, expected rate extraction, and scenarios with prescribed flight control and environmental conditions [7], [8]. In [9], empirical mode decomposition, which relies on prior knowledge of the desired signal, was proposed to compensate for the motion of the platform. Other self-compensation techniques for radar movement have been proposed using different methods to obtain a reference signal to cancel the noise. For example, frequency-modulated continuous wave (FMCW) [10] and ultrawideband (UWB) [11] radars with range discrimination were used to capture radar motion signals relative to stationary clutter. In [12] and [13], a dual-frequency radar was used to capture radar motion signals obtained with a stationary reflector, and the

Received 21 February 2025; revised 23 April 2025; accepted 12 May 2025. This work was supported in part by the National Science Foundation (NSF) under Grant IIS1915738 and Grant CNS2039089, in part by the DoD SMART Scholarship, and in part by the Naval Innovative Science and Engineering (NISE) Program under Contract N660011924706. *(Corresponding author: Khaldoon M. Ishmael.)*

This work involved human subjects or animals in its research. Approval of all ethical and experimental procedures and protocols was granted by the Institutional Review Board (IRB) of the University of Hawai'i Human Studies Program ("Remote Sensing of Physiological Motion Using Doppler Radar" Protocol) under Application No. CHS 14884.

Khaldoon M. Ishmael and Richard C. Ordoñez are with the Naval Information Warfare Center, Pearl City, HI 96782 USA (e-mail: khaldoon.m.ishmael.civ@us.navy.mil; richard.c.ordonez.civ@us.navy.mil).

Shekh M. M. Islam is with the Department of Electrical and Electronic Engineering, University of Dhaka, Dhaka 1000, Bangladesh (e-mail: mahmud@du.ac.bd).

Mohammad Shadman Ishrak, Jannatun Noor Sameera, Victor M. Lubecke, and Olga Borić-Lubecke are with the Department of Electrical and Computer Engineering, University of Hawai'i at Mānoa, Honolulu, HI 96822 USA (e-mail: ishrak@hawaii.edu; jsameera@hawaii.edu; lubecke@hawaii.edu; olgabl@hawaii.edu).

Digital Object Identifier 10.1109/TMTT.2025.3570603

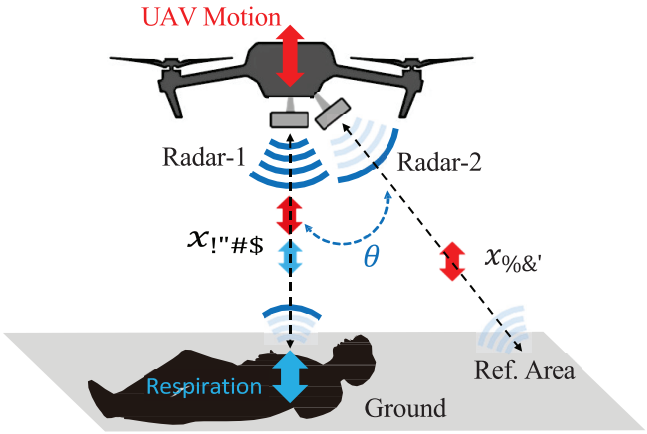

Fig. 1. DRNC system framework involves Radar 1 as the main input, positioned beneath the UAV to detect the chest movements of the target and associated noise. Radar 2, functioning as the reference input, is situated at θ to Radar 1, capturing solely the noise signal.

desired signal was recovered using adaptive noise cancellation (ANC). A single and multiple FMCW radars mounted on a moving platform was used to cancel radar motion based on different range and velocity observations of a target due to their spatial distribution for SAR imaging [14], [15]. A dual continuous wave (CW) radar system for ANC of UAV platform motion was proposed in [16] and demonstrated through simulations using a robotic mover to replicate flight vibrations of the UAV and breathing motions. Previous radar-based motion compensation approaches were not tested on a flying UAV [10], [11], [16], and ANC-based methods [12], [13], [16] used a linearly demodulated reference signal which limited their application to a smaller range of motion and recovery of motion rates only. This work proposes and experimentally demonstrates two dual radar-based noise cancellation (DRNC) approaches that use arctangent demodulated reference signals, enabling compensation of a larger motion and accurate recovery of respiratory rate and displacement for a UAV-born system. The approach robustly preserves an accurate measurement of the time-varying displacement even in scenarios where the UAV undergoes an arbitrary turbulent displacement of more than an order of magnitude greater than that of the respiratory motion. This type of system provides significant advancement since displacement measurements are suitable for advanced analytics, including respiratory airflow, separation of multiple subjects, and authentication of the identity of the subject [17], [18].

A fully radar-based UAV motion compensation system is presented here, as applied to simulated flight and in-flight radar measurements of a robotic respiratory mover and actual human respiration. Fig. 1 shows the outdoor setup of the DRNC, which includes both radars mounted under the frame of the UAV. This setup relies on a reflection from a stationary ground to provide a reference signal, which is usually accessible for land-based applications; the primary input, Radar 1, is located directly beneath the UAV and is tasked with detecting the target's chest movements along with any associated noise. Radar 2 acts as the reference input; it is positioned at an angle θ to Radar 1 and is specifically designed to capture only the noise signal. The reference signal, denoted as x_{ref}, can be mathematically expressed as

$$x_{\text{ref}} = x_{\text{noise}} \times \cos(\theta). \tag{1}$$

This article is structured as follows. Section II outlines the theoretical basis for employing arctangent demodulation to achieve precise radar assessments of torso movement during breathing. Section III introduces two methods, ANC and net signal interference cancellation (NIC), which contribute to the dual-radar noise cancellation (DRNC) function. Section IV details the design and implementation of a UAV-based DRNC system characterized by its small size, weight, and power or cost efficiency (SWaP-C). Section V presents experimental results related to displacement and rate signatures of both a robot and a human subject, successfully showcasing the airborne detection of target breathing rate and displacement with high precision. To the best of our knowledge, this is the first demonstration of ANC using arctangent demodulated signals to enable accurate displacement measurements in the presence of large motion and the first UAV flight using DRNC to measure human respiration rate and displacement with high accuracy.

II. Doppler Radar Phase Demodulation

Based on the Doppler theory, a target with a time-varying position with no net velocity will reflect a signal with phase modulation, which is proportional to the target's time-varying position. A CW Doppler radar signal is transmitted toward a target from which it is partly reflected to the receiving antenna. A quadrature receiver with in-phase (I) and quadrature (Q) channels is typically used for optimal sensitivity [19]. The reflected signal phase in each channel is measured and compared to the transmitted signal. The resulting phase difference is due to variations in the round-trip travel time of the signal reflected by the target. The chest movements of the human subject generate a periodic displacement with no net velocity. Demodulating the phase of the periodic motion signal provides information directly related to chest displacement due to respiration. The following equation can represent the CWtransmitted signal:

$$T(t) = A\cos(\omega t + \phi(t)) \tag{2}$$

where A is the amplitude, ω_0 is the radio oscillation frequency of the transmitted signal, and $\phi(t)$ is the oscillator phase noise, representing the fluctuation of the random phase within the oscillator. The receiving antenna captures the backscattered portion of the signal with changes in phase and amplitude. The quadrature baseband output signals received can be expressed as

$$B_I(t) = A_r\cos\left(\phi + \frac{4\pi x(t)}{\lambda} + \Delta\phi(t)\right) \tag{3}$$

and

$$B_Q(t) = A_r\sin\left(\phi + \frac{4\pi x(t)}{\lambda} + \Delta\phi(t)\right) \tag{4}$$

where A_r is the received signal amplitude, λ is the wavelength, ϕ is the constant phase shift caused by the reflection surface and the time delay between the transmitter and the antenna

and between the antenna and the mixer, and $\Delta\phi(t)$ is the residual phase noise, and $x(t)$ is the movement of the target. Previous ANC work used linear demodulation [12], [13], [16], which limited motion cancellation to small motion and signal recovery to motion rates. In this work, arctangent demodulation is used to achieve accurate phase demodulation and displacement recovery regardless of the target position and motion amplitude [19]. The received signal phase $\phi(t)$ is the result of combining the received quadrature baseband outputs (2) and (3). It can be expressed as follows:

$$\phi(t) = \arctan\left(\frac{B_Q(t)}{B_I(t)}\right). \tag{5}$$

When applying arctangent demodulation to the quadrature outputs, it is essential to compensate for the quadrature channel imbalance between the I and Q outputs, remove the unwanted dc offset, and perform signal phase unwrapping. These demodulation steps are illustrated for the 24 GHz radar data taken with the commercial off-the-shelf (COTS) RF-beam Microwave K-MC1 module [20]. This module consists of a dual 30-patch K-band antenna array with a beam aperture of 25° × 12° and an antenna gain of 16 dBi. The transmit output power is 16.5 dBm. The receiver includes a quadrature down-converter with dc-coupled I and Q outputs, facilitating accurate respiration measurements. The module has dimensions of 65 × 65 × 6 mm, and it weighs 50 g. The frequency of 24 GHz was selected to ensure compact hardware and minimize propagation loss. Radar signal at 24 GHz can penetrate foliage effectively and generate a significant ground reflection, used as a reference signal, as illustrated in Fig. 1. The target is mounted on a translation stage that oscillated along one axis at a frequency of 0.2 Hz with a peak-to-peak amplitude movement of 5 mm. The arctangent demodulation of the baseband output waveform with IQ channel imbalance and dc offset correction can be expressed as

$$\phi(t) = \arctan\left(\frac{\mathrm{dc}_Q + A_e \sin\ (\theta + \varphi_e + p(t))}{\mathrm{dc}_I + \cos(\theta + p(t))}\right) \tag{6}$$

where dc_Q and dc_I are the dc offsets of the output of the quadrature channel, the amplitude and phase error are A_e and φ_e, respectively, and the phase $p(t)$ is related to the target motion $(4\pi\Delta x(t)/\lambda)$. The IQ channel imbalance ratio occurs when the phase difference is not precisely 90 and the amplitude attenuation values are mismatched [21], [22]. The amplitude mismatch produces a major and minor axis along the path of the arc, essentially creating an ellipse. The ellipse can be expressed by the general equation

$$AI^2 + BIQ + CQ^2 + DI + EQ + F = 0. \tag{7}$$

The imbalance factors of the ellipse can be expressed as:

$$A_e = \frac{1}{\sqrt{|A|}} \tag{8}$$

$$\phi_e = -\arcsin\left(\frac{B}{2A_e}\right) \tag{9}$$

where A_e and ϕ_e are the amplitude imbalance and phase imbalance factors, respectively.

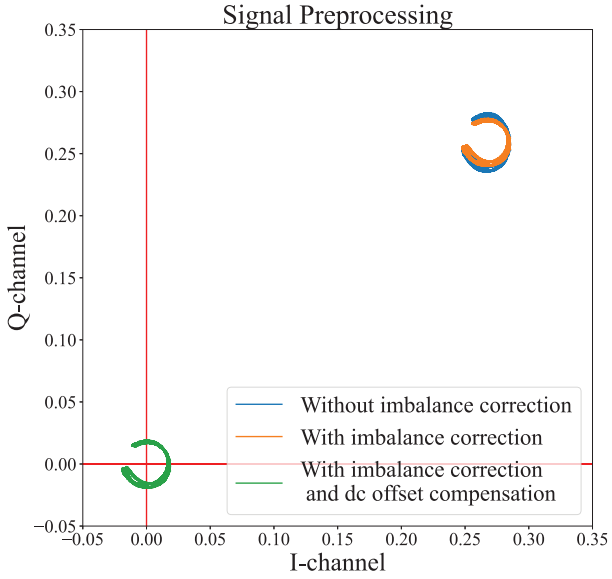

Fig. 2. 24 GHz radar assessment of a mechanical target oscillating at a frequency of 0.2 Hz, exhibiting a peak-to-peak displacement of 5 mm. The IQ plot depicts three pre-processed traces: the unaltered data, the data adjusted for imbalance, and the data further refined with dc offset correction.

The Gram-Schmidt procedure is used for the known compensation for phase and amplitude imbalance [23]. The Gram-Schmidt procedure can transform the imbalanced signals into orthonormalized signals with known imbalance values. The orthonormalized signals can be expressed as

$$I_{\mathrm{orth}} = I \tag{10}$$

$$Q_{\mathrm{orth}} = -\tan(\phi_e)I + \frac{Q}{A_e\cos(\phi_e)}. \tag{11}$$

The IQ plot in Fig. 2 illustrates the demodulation correction steps applied to the recorded dataset.

The true displacement amplitude of the signal is 5 mm, peak to peak. Without dc offset compensation, the arctangent demodulated signal's maximum phase change is, however, lower, decreasing the displacement amplitude information derived from the phase information, as illustrated in Fig. 3(a). The dc offset is caused by signal leakage in the direct conversion system and clutter reflections from the external environment. After removing the dc offset, the quadrature outputs center around the zero-amplitude line. This can be achieved by taking the signal's average to get the dc offset values and subtracting these values from the original signals, as illustrated in Fig. 3(b).

After imbalance compensation and dc offset correction, the phase response can be expressed as follows:

$$\phi(t) = \arctan\left(\frac{\sin(\phi + p(t))}{\cos(\phi + p(t))}\right) = \phi + p(t). \tag{12}$$

The signal exceeds $+-\pi/2$, making the phase distribution discontinuous [24]. Phase unwrapping is, therefore, needed to make the phase distribution continuous to recover the correct response. Fig. 3(b) illustrates the signal before phase unwrapping, and Fig. 3(c) illustrates the signal phase unwrapping, with a 5 mm peak-to-peak displacement amplitude.

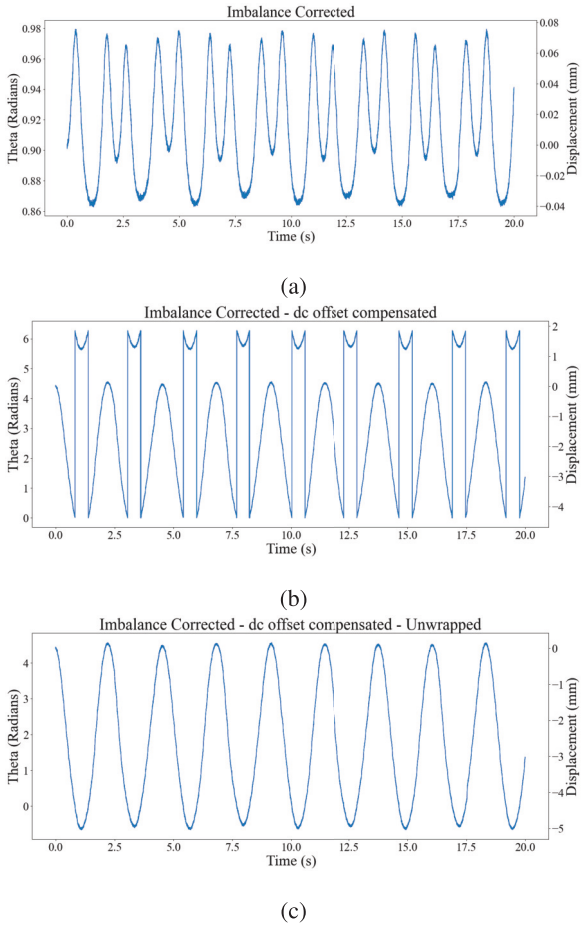

Fig. 3. (a) Phase of the 24 GHz radar output signal in the time domain, following the correction for channel imbalance. The displacement amplitude remains minimal as a result of a substantial dc offset. (b) Compensation for both channel imbalance and dc offset is applied. Because the phase range surpasses $+-\pi/2$, the demodulated phase exhibits discontinuities. (c) Unwrapped data of the signal phase for the quadrature outputs. The measured displacement accurately corresponds to the actual 5-mm peak-to-peak amplitude.

III. Interference Canceler Techniques

Two interference cancellation techniques were explored as a means of taking advantage of dual radar system output: net signal interference cancellation (NIC) and ANC. Assuming that the detected target motion signal is (x_{des}) and the interference noise from the UAV platform is (x_{noise}), the combined captured signal can be expressed as (x_{com}).The noise signal (x_{noise}) must be reduced to recover the desired signal (x_{des}) successfully.

Fig. 4 shows a dual-radar framework that incorporates both a primary and a reference input. The system captures a total signal indicated as (x_{com}), which includes the respiration signal resulting from chest movement (x_{des}) and the noise signal (x_{noise}). Te reference input, moreover, records only the noise signal (x_{ref}) from a reflective surface, such as the ceiling or floor.

The NIC method is used to isolate the desired signal using the opposing interference noise signal. By combining the primary and reference inputs, the interference caused by the noise signal is subtracted, thus isolating the desired signal. Since arctangent demodulation is used to recover absolute

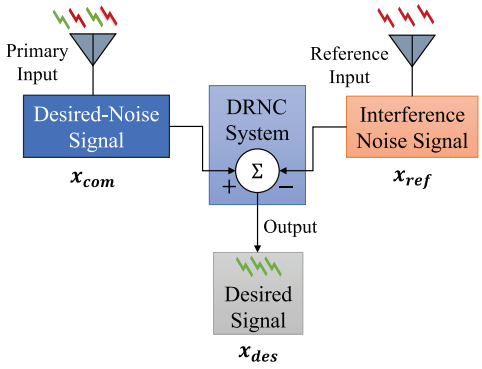

Fig. 4. Diagram of the DRNC system displaying both primary input and reference input.

displacement, it is not necessary to scale the received signal strength due to different path lengths for Radars 1 and 2. The recovered Radar 2 displacement should, however, be scaled in the direction of Radar 1 to obtain the reference for the UAV motion in the desired direction. The desired signal x_{des} can be mathematically expressed and obtained from the following equations:

$$x_{\text{com}} = x_{\text{des}} + x_{\text{noise}} \tag{13}$$

$$x_{\text{noise}} = x_{\text{ref}} \div \cos(\theta) \tag{14}$$

and

$$x_{\text{des}} = x_{\text{com}} - x_{\text{noise}}. \tag{15}$$

The ANC method uses an adaptive filter to effectively eliminate noise signals Fig. 5. Unlike conventional filters, which use fixed coefficients to meet specific objectives such as attenuating all frequencies above a designated cutoff frequency [25], adaptive filters have coefficients that change dynamically. This adaptability allows the filter to converge toward an optimal state. The design of these filters typically involves selecting coefficients that best approximate the desired frequency response [25], [26]. The performance of the adaptive filter is evaluated using a cost function, commonly the mean square of the error signal between the output of the adaptive filter and the intended signal. As filter coefficients are adjusted, the mean square error (mse) decreases and approaches its minimum value [26]. The primary input receives a signal s distorted by uncorrelated noise, n. Meanwhile, the reference input captures a noise signal n_0, which is not correlated with s but is related to noise n. The signal n_0 is filtered to produce an output $\acute{n}$, which closely approximates the noise n. This noise estimate is then subtracted from the distorted signal to yield an estimate of the original signal, $\acute{s}$. The ANC system generates the following outputs:

$$\acute{s} = s + n - \acute{n} \tag{16}$$

and

$$\acute{s}^2 = s^2 + (n - \acute{n})^2 + 2s(n - \acute{n}) \tag{17}$$

taking long-term averages on both sides and assuming that $\acute{s}$ is not correlated with the source signal:

$$\begin{aligned} E[\acute{s}^2] &= E[s^2] + E[(n - \acute{n})^2] + E[s(n - \acute{n})] \\ &= E[s^2] + E[(n - \acute{n})^2] \end{aligned} \tag{18}$$

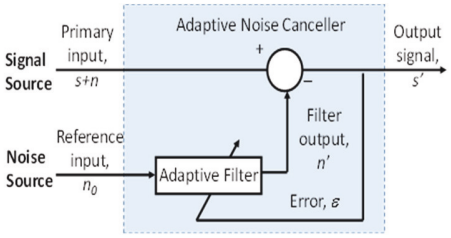

Fig. 5. Block diagram demonstrates the general approach of the ANC method [14].

the basic adaptive filtering technique is based on modifying the filter coefficients to minimize $E[\acute{s}^2]$ while keeping the signal strength $E[s^2]$ constant

$$\min E[\acute{s}^2] = E[s^2] + \min E[(n - \acute{n})^2] \tag{19}$$

for minimizing $E[\acute{s}^2]$ there are two prominent algorithms: least mean squares (LMSs) and RLSs [25], [26]. An LMS filter attempts to modify its coefficients according to the smallest discrepancies between the desired signal and the actual signal [25], [26]. In contrast, RLS iteratively determines the filter coefficients that minimize the weighted linear least squares cost function of the input signals [25], [26]. The RLS filter updates the filter coefficients by using the equation below

$$w(n+1) = w(n) + e(n)k(n) \tag{20}$$

where $w(n)$ is the filter coefficient, $e(n)$ is the error signal or difference between the input and the desired signal, and $k(n)$ is the gain vector defined by the following equations:

$$k(n) = P(n)U(n)/(\lambda + U^T(n)P(n)U(n)) \tag{21}$$

and

$$U(n) = (r(n)r(n-1), \ldots, r(n-N+1)) \tag{22}$$

where λ is the forgetting factor, N is the filter order, and $P(n)$ is the inverse correlation matrix of the input noisy signal with the following initial value $P(0)$:

$$P(0) = \delta^{-1} I_N, \quad 0 < \delta \ll 1 \tag{23}$$

the standard recursive least square (RLS) algorithm uses the below equation to update the correlation matrix

$$P(n+1) = \lambda^{-1}P(n) - \lambda^{-1}k(n)U^T(n)P(n). \tag{24}$$

The DRNC system used the RLS algorithm because of its iteration capabilities to update the filter coefficients that generally help to better estimate the original signal from the noisy signal. Arctangent demodulation is used to produce a reference signal for RLS, enabling accurate displacement recovery.

Fig. 6 shows the indoor setup of the DRNC, which features the primary input, Radar 1, located directly below the UAV frame and is tasked with detecting the target's chest movements along with any associated noise. The reference input Radar 2, positioned at a $\theta = 180°$ angle to Radar 1, directly on the top of the UAV frame, captures only the noise signal reflected from the ceiling. The UAV position between the target and the ceiling does not need to be controlled since recovered displacement using arctangent demodulation does

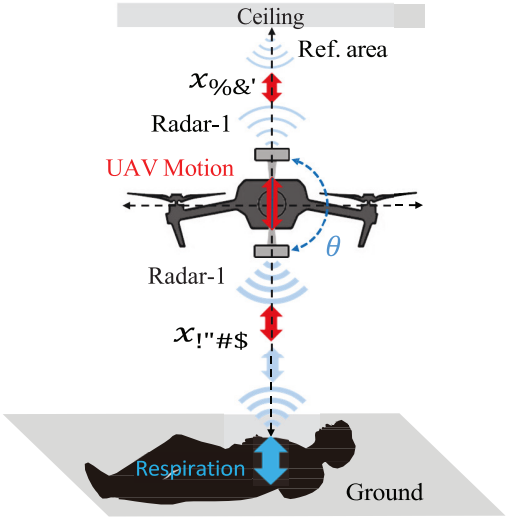

Fig. 6. UAV is equipped with two radar systems. Radar 1, installed on the bottom, captures both the target's chest movements and environmental noise. In contrast, Radar 2, mounted on top, records merely the noise signal.

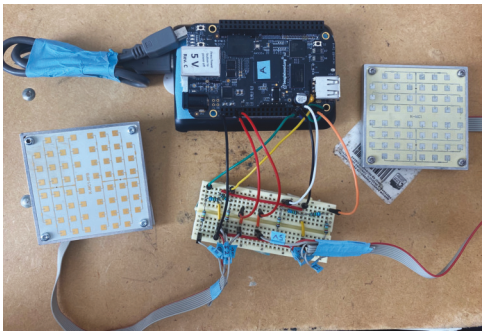

Fig. 7. This photograph displays the components of the DRNC system. The K-MC1 radars were linked to signal conditioning circuits and the BBB. The entire setup was powered by a portable battery situated beneath the BBB.

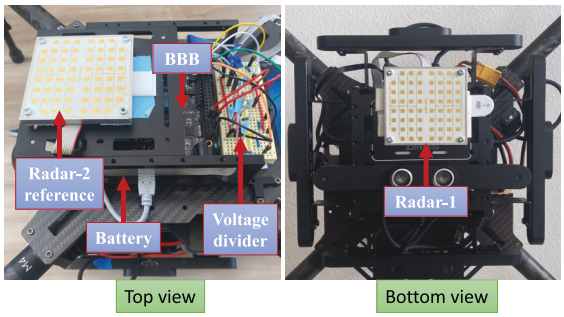

Fig. 8. Photograph displays the DRNC system installed on the UAV. From the top view, it includes Radar 2, BBB, a voltage divider, and a battery, while the bottom view features Radar 1.

not rely on received signal strength. The noise signal, denoted as x_{noise}, can be mathematically expressed as

$$x_{\text{noise}} = -x_{\text{ref}}. \tag{25}$$

IV. Architecture of the DRNC System

The DRNC system is designed to be both rigid and lightweight, weighing approximately 350 g. It consists of two 24 GHz K-MC1 radar modules [20], the BeagleBone Black (BBB) development platform for data acquisition, a portable

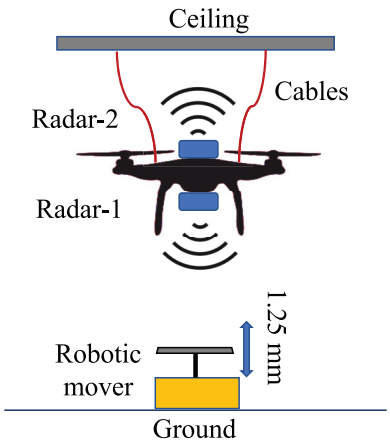

Fig. 9. Initial demonstration of UAV simulation flight tests involved a UAV being vertically suspended from the ceiling using bungee cords.

lithium battery, and a signal conditioning board. The radar modules do not cause interference due to range correlation [27] since only received signals that originate from the same source as a transmit signal will produce a useful output signal. Signals from other sources will be uncorrelated and will not obscure desired signals unless they saturate the receiver. Since reflections from the second radar mounted at some angle from the first radar will be lower in magnitude, saturation is, however, not likely to occur. The BBB uses the TI Sitara AM335 × 1 GHz ARM Cortex A8 processor for analog-to-digital conversion and signal recording [28]. The DRNC system is powered by a portable lithium battery with a capacity of 4000 mAh. The BBB requires a positive input to the ADC with a maximum voltage amplitude of 1.8 V. In order to meet this requirement, a custom signal conditioning circuit with an additional dc offset was implemented between the radar output and the BBB, ensuring that a suitable input signal is provided to the ADC. Fig. 7 displays a photograph of the hardware components of the DRNC. The experiment was carried out using a DJI Matrice 100 quadcopter. The payload was neutrally positioned at the center of gravity of the platform to avoid any impact on flight performance. Fig. 8 provides photographs showing the DRNC mounted and attached to the UAV, which presents views from both the top and the bottom.

A customized Python program was uploaded to the BeagleBone Black (BBB) to initiate the recording of the board's analog channels, specifying the start and end times. The sampling frequency was set at f_s = 685.7 Hz. The data acquired by Radars 1 and 2 were stored in the BBB via a microSD card. After landing the UAV, a MATLAB program was used to collect the data from the microSD card for postprocessing. Noise cancellation and arctangent demodulation algorithms were employed to extract the desired signal.

V. Experimental Results

The DRNC system mounted on the UAV was tested using a mechanical target and a human subject. The initial testing was carried out by suspending the UAV from a ceiling using bungee cords, as illustrated in Fig. 9. Radar-2 was placed on top of the UAV platform approximately four feet away from the ceiling, and radar-1 was placed on the bottom of the UAV platform approximately four feet away from the robotic mover placed on the ground. A noise motion signal was manually introduced to the UAV platform to simulate a hovering flight scenario. The robotic mover simulated a repetitive respiration motion to obtain reproducible results before flying. Under normal conditions, the human respiratory rate is between 12 and 18 breaths per minute, which corresponds to a breathing rate between 0.2 and 0.3 Hz. The rectangular plate is mounted vertically on a translation liner stage with one motion axis. The Griffin Motion LNS-100 series linear stage platform was operated through a Galil DMC30010 controller, which was engaged using a stepper drive managed through a serial interface. In this test, the robotic mover oscillated with a frequency rate of 0.3 Hz. The displacement amplitude tested was 1.25 mm peak-to-peak (test-1) and 5 mm peak-to-peak (test-2). The target amplitude displacement D_{amp} can be estimated from the signal phase $\phi(t)$ after applying noise cancellation techniques and arctangent demodulation

$$D_{\text{amp}} = \frac{\phi(t)\lambda}{4\pi}. \tag{26}$$

The displacement estimation algorithm used the peak finding algorithm to identify the peaks and valleys. The average of valleys was subtracted from the average of peaks to obtain the average displacement. The error rate of the estimated displacement is assessed as follows:

$$\text{Error rate } (\%) = \left(\frac{|x_{\text{est}} - x_{\text{act}}|}{x_{\text{act}}}\right) \times 100 \tag{27}$$

where x_{est} and x_{act} are the estimated and actual displacement, respectively. Table I summarizes the estimated displacement and the error percentage for both tests. Displacement amplitude was measured with an error of less than 3% for 5-mm displacement and with an error of less than 10% for 1.25-mm displacement with both NIC and ANC methods.

TABLE I
Suspended UAV Robotic Mover Displacement Recovery

Test	Actual [mm]	NIC [mm]	Error [%]	ANC [mm]	Error [%]
T1	1.25	1.14	8.8	1.13	9.5
T2	5	5.11	2.2	5.08	1.6

The DRNC system was tested on an airborne UAV for both a robotic mover and a human subject. While hovering, the UAV maintained a steady position above a target. During all test scenarios, the hover duration over the target was 100 s.

A. Detection of Robotic Mover Motion

The human respiration model was simulated using a robotic mover representing human chest motion, as shown in Fig. 10. The frequencies tested were 0.2 Hz (test-1) and 0.3 Hz (test-2). The robotic mover oscillated with a peak-to-peak amplitude of 10 mm in both tests.

In time-domain analysis, the overall data collected from radar-1 and radar-2 represents the vertical motion of the UAV in opposite directions; therefore, when the radar-1 signal

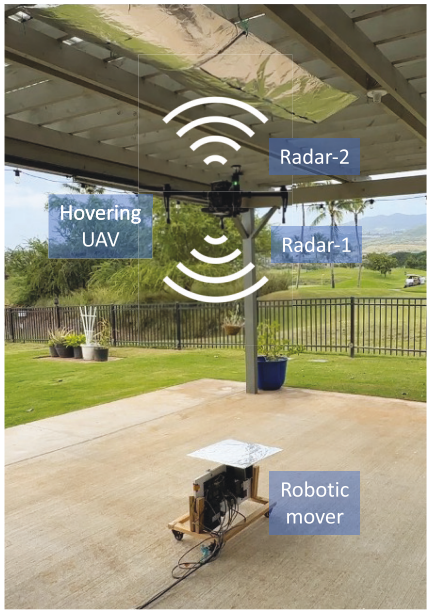

Fig. 10. Image captures the UAV flying above the automated mover. Radar 2 was about four feet below the ceiling, with Radar 1 positioned roughly four feet away from the mover.

TABLE II
FLYING UAV ROBOTIC MOVER DISPLACEMENT RECOVERY

Test	Actual [mm]	NIC [mm]	Error [%]	ANC [mm]	Error [%]
T1	10	9.77	2.27	9.74	2.56
T2	10	10.44	4.43	10.14	1.42

shows a valley, the radar-2 signal shows a peak, and vice versa. The desired signal from the mover x_{des} was recovered using NIC and ANC techniques. Fig. 11 illustrates the demodulated arctangent outputs in the time and frequency domain for the test data captured by radar 1 (a) and radar 2 (b) before applying interference cancellation techniques.

Fig. 12 illustrates the outcome of the NIC technique. This approach eliminates the interference noise by combining the primary radar signal 1 with the reference input signal radar 2, thereby allowing the desired signal at 0.3 Hz to be distinguished as the most prominent peak above 0.1 Hz (corresponding to robotic mover motion).

The outcome of the ANC method is depicted in Fig. 13. This method uses radar 2 as a reference input to create an estimated signal that closely approximates the target signal. It adjusts the filter coefficients to reduce noise while maintaining the consistent strength of the desired signal. Like the NIC method's results, the ANC output features a distinct peak at 0.3 Hz.

The frequency-domain analysis identifies a notable peak at lower frequencies, which can be attributed to Beaglebone's microprocessor and issues in grounding design. The NIC and ANC methods effectively retrieved the oscillation frequency of the target signal, as shown in Figs. 12 and 13. The displacement estimation algorithm was used on the NIC and ANC data at 0.2 and 0.3 Hz to determine the signal's displacement amplitude. Table II presents the estimated displacement

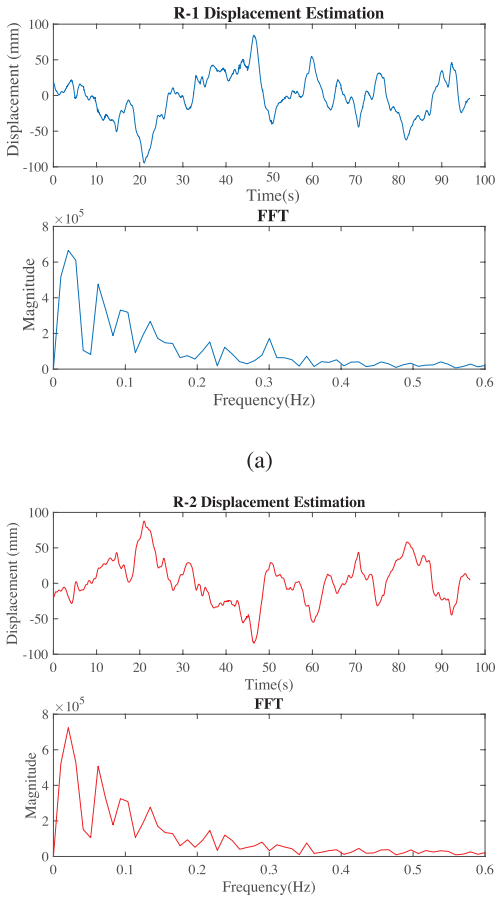

Fig. 11. Results from UAV airborne tests in both time and frequency domains, conducted with a robotic mover oscillating at 0.3 Hz and achieving a peakto-peak displacement of 10 mm, are presented for (a) radar 1 and (b) radar 2.

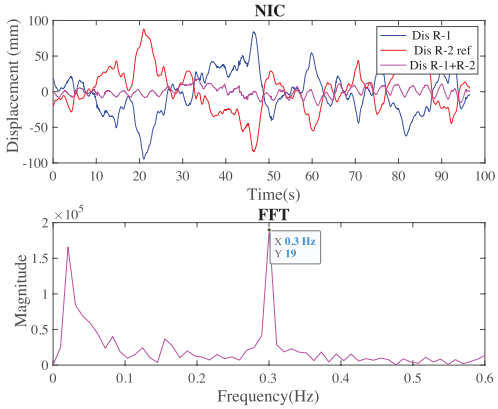

Fig. 12. In the time and frequency domains, the NIC output signal is observed while a UAV hovers above a mechanical target that oscillates at a frequency of 0.3 Hz with a 10 mm peak-to-peak displacement. The frequency-domain analysis of the expected signal reveals a distinct peak at 0.3 Hz.

recovery along with the percentage error for each method. In all instances, the displacement was retrieved with an error below 5%.

B. Detection of Human Respiration Waveform

The human testing for this study adhered to the protocol number 14884 outlined by the Committee on Human Studies

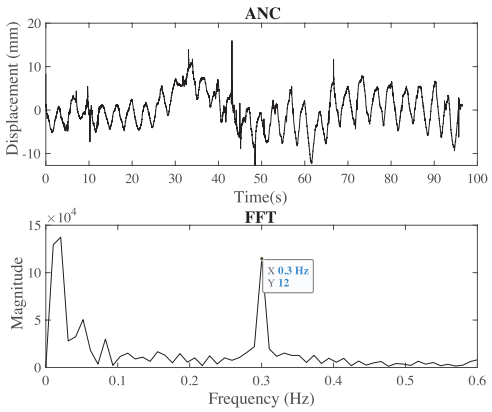

Fig. 13. ANC output signal is presented in both the time domain and frequency domain for a UAV hovering above a robotic mover. The mover oscillates at a frequency of 0.3 Hz with a peak-to-peak displacement of 10 mm.

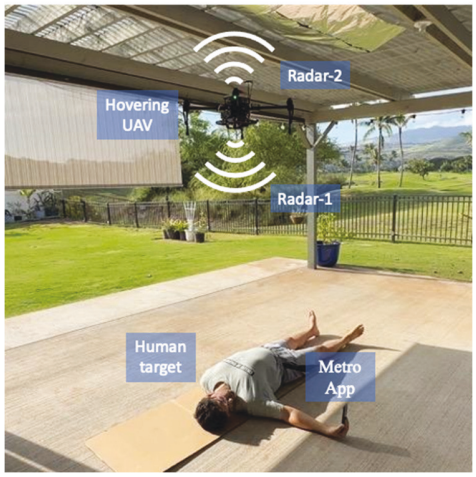

Fig. 14. Image shows a UAV flying over a human target. Radar-2 is roughly four feet beneath the ceiling, while radar-1 is around four feet away from the individual.

TABLE III
HUMAN CHEST MOTION FREQUENCY/DISPLACEMENT RECOVERY

Test	Measured [Hz]	Actual [Hz]	NIC [mm]	ANC [mm]
T1	0.2	0.2	5.5	5.2
T2	0.3	0.3	5.9	5.3

(CHS), with approval granted by the University of Hawai'i system's CHS. As depicted in Fig. 14, the subject was positioned on the ground in the same orientation where the robotic mover originally sat. Breathing rates of 0.2 and 0.3 Hz were evaluated using a metronome program serving as a breathing guide.

Fig. 15(a) and (b) illustrate the demodulated arctangent data obtained from radars 1 and 2. As with the data from the robotic mover results, a significant peak is observed at lower frequencies, which can be attributed to the BeagleBone's microprocessor architecture+.

Interference cancellation techniques were used to remove noise and enhance the amplitude of the target signal. Figs. 16 and 17 present the results in both the time and frequency domains for the NIC and ANC approaches. In both cases, the

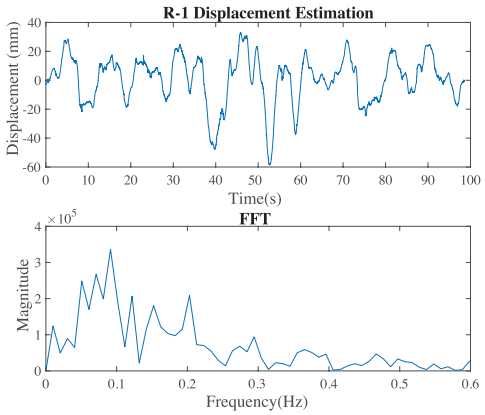

(a)

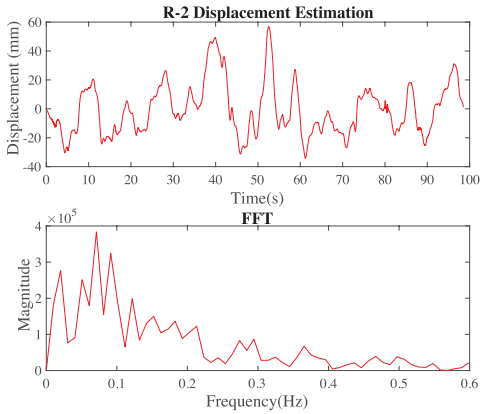

(b)

Fig. 15. For a human subject with a breathing rate of 0.2 Hz, the airborne test results using UAVs are shown for (a) radar-1 and (b) radar-2 in both time and frequency domains.

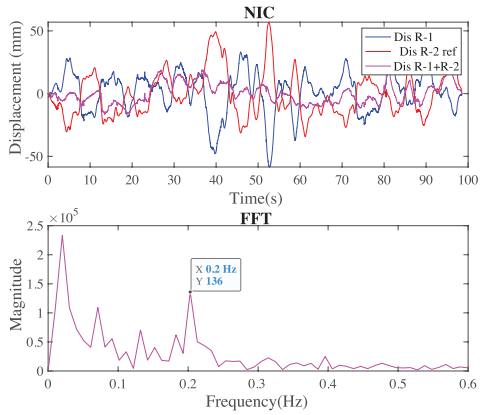

Fig. 16. NIC output signal when a UAV is stationary over a human subject exhibiting a breathing rate of 0.2 Hz is displayed in both the time domain and the frequency domain.

noise was significantly diminished, allowing the target signal to stand out at the breathing frequency of 0.2 Hz.

Table III presents a comparison between the measured breathing frequency, the metronome frequency, and the breathing displacement derived from the NIC and ANC outputs at both breathing frequencies. In both instances, the breathing frequency was precisely measured. The percentage displacement error was not computed due to the lack of a reference

TABLE IV
COMPARISON OF UAV IN-FLIGHT RESPIRATION MEASUREMENTS

Ref	Proposed system	Operating frequency	Experimental method	Proposed method	Respiration rate accuracy	Displacement accuracy
4	CW radar with ultrasonic, camera and IMU sensors	10.5 GHz	UAV hovering over mechanical target	Motion compensation algorithm with a Platform Stabilization PID feedback loop	NA	NA
5	FMCW radar and a LIDAR system	77 GHz with chirp bandwidth of 1 GHz	UAV flown in a room, seated human subject	LIDAR and reflections from stationary objects used for motion compensation	1.3 %	NA
7	SAR-imaging system with FMCW radar	5.8 GHz with a bandwidth of 320 MHz	Prescribed trajectory, standing subject	SAR imaging with FMCW trajectory extraction	NA	NA
8	UWB radar with onboard camera reference	7.29 GHz with a bandwidth of 1.4 GHz	UAV hovering over supine human subject	Platform motion compensation based on range profile with static platform and background	10 %	NA
This work	Dual CW radar	24 GHz	UAV hovering over supine human subject	DRNC configuration with ANC and NIC methods	1 %	3 % - 10 %

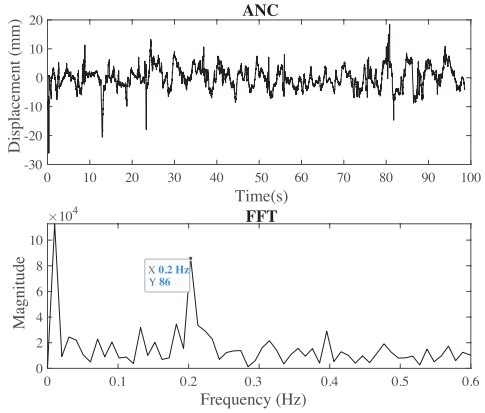

Fig. 17. ANC output signal is examined in both the time domain and frequency domain while the UAV hovers over a human subject with a breathing rate of 0.2 Hz.

measurement of the human chest's displacement. The obtained breathing displacement is, nonetheless, within the anticipated range.

Table IV shows the comparison of published results for UAV-mounted radar flight measurements of physiological motion. Respiratory rate was successfully obtained with errors within 10% and 1.3% with UAV-based UWB [8] and FMCW [5] radar systems. Both systems depend on platform motion compensation that relies on additional optical sensors and requires extensive postprocessing. In this work, respiratory rate was recovered with accuracy within 1% with a less computationally intensive approach that can be implemented in near real-time. In addition, this is the first demonstration of respiratory waveform recovery from a flying UAV, with a respiratory displacement error of less than 10%. Respiration displacement error was a fraction of 1 mm even in the presence of platform motion exceeding 100 mm.

VI. CONCLUSION

A dual-radar noise compensation (DRNC) system has been proposed and has been shown to be effective for the detection of physiological signals and displacements from a UAV platform. The study examined two interference cancellation methods, NIC and ANC, aimed at reducing motion interference from the UAV platform. Arctangent demodulation reference signals were used for NIC and ANC, enabling compensation of large motion and accurate displacement measurements. The theoretical basis for the cancellation techniques was established and validated through a combination of laboratory simulations and UAV flight tests with a 24 GHz DRNC system. Across all testing conditions, which included trials with both mechanical targets and human subjects, frequency and displacement measurements were recorded with high precision. Errors in these measurements were maintained below 1% and 10%, respectively. To the best of the authors' knowledge, this is the first demonstration of ANC using arctangent demodulated signals to enable accurate displacement measurements in the presence of large motion, and the first UAV flight using DRNC to measure human respiration rate and displacement with high accuracy. Future work integrating real-time search and localization using respiration cues remains an important next step in our research, and we are actively exploring strategies to enhance detection and localization capabilities in more dynamic environments.

REFERENCES

[1] C. E. Lin and S.-K. Yang, "Camera gimbal tracking from UAV flight control," in *Proc. CACS Int. Autom. Control Conf. (CACS)*, Nov. 2014, pp. 319–322.

[2] Y. Rong, R. Gutierrez, K. V. Mishra, and D. W. Bliss, "Noncontact vital sign detection with UAV-borne radars: An overview of recent advances," *IEEE Veh. Technol. Mag.*, vol. 16, no. 3, pp. 118–128, Sep. 2021.

[3] B. P. A. Rohman, D. Kurniawan, C. B. Ali Wael, and A. Subekti, "Toward a compact and reconfigurable radar-UAV for remote vital sign detection," in *Proc. Int. Conf. Radar, Antenna, Microw., Electron., Telecommun. (ICRAMET)*, Dec. 2022, pp. 68–72.

[4] R. H. Nakata, B. Haruna, T. Yamaguchi, V. M. Lubecke, S. Takayama, and K. Takaba, "Motion compensation for an unmanned aerial vehicle remote radar life sensor," *IEEE J. Emerg. Sel. Topics Circuits Syst.*, vol. 8, no. 2, pp. 329–337, Jun. 2018.

[5] P. Stockel, P. Wallrath, R. Herschel, and N. Pohl, "Detection and monitoring of people in collapsed buildings using a rotating radar on a UAV," *IEEE Trans. Radar Syst.*, vol. 2, pp. 13–23, 2024.

[6] P. Stockel, P. Wallrath, R. Herschel, and N. Pohl, "Motion compensation in six degrees of freedom for a MIMO radar mounted on a hovering UAV," *IEEE Trans. Aerosp. Electron. Syst.*, vol. 59, no. 5, pp. 5791–5801, Oct. 2023.

[7] J. Yan, Z. Peng, H. Hong, H. Chu, X. Zhu, and C. Li, "Vital-SAR-imaging with a drone-based hybrid radar system," *IEEE Trans. Microw. Theory Techn.*, vol. 66, no. 12, pp. 5852–5862, Dec. 2018.

[8] J. Yan, G. Zhang, H. Hong, H. Chu, C. Li, and X. Zhu, "Phase-based human target 2-D identification with a mobile FMCW radar platform," *IEEE Trans. Microw. Theory Techn.*, vol. 67, no. 12, pp. 5348–5359, Dec. 2019.

[9] S. M. M. Islam, L. Oba, and V. M. Lubecke, "Empirical mode decomposition (EMD) for platform motion compensation in remote life sensing radar," in *Proc. IEEE Radio Wireless Symp. (RWS)*, Jan. 2022, pp. 41–44.

[10] Y. Rong, A. Herschfelt, J. Holtom, and D. W. Bliss, "Cardiac and respiratory sensing from a hovering UAV radar platform," in *Proc. IEEE Stat. Signal Process. Workshop (SSP)*, Jul. 2021, pp. 541–545.

[11] E. Cardillo, C. Li, and A. Caddemi, "Vital sign detection and radar self-motion cancellation through clutter identification," *IEEE Trans. Microw. Theory Techn.*, vol. 69, no. 3, pp. 1932–1942, Mar. 2021.

[12] A. Singh and V. Lubecke, "Adaptive noise cancellation for two frequency radar using frequency doubling passive RF tags," *IEEE Trans. Microw. Theory Techn.*, vol. 61, no. 8, pp. 2975–2981, Aug. 2013.

[13] F. Zhu, K. Wang, and K. Wu, "A fundamental-and-harmonic dual-frequency Doppler radar system for vital signs detection enabling radar movement self-cancellation," *IEEE Trans. Microw. Theory Techn.*, vol. 66, no. 11, pp. 5106–5118, Nov. 2018.

[14] M. Steiner, T. Grebner, and C. Waldschmidt, "Millimeter-wave SAR-imaging with radar networks based on radar self-localization," *IEEE Trans. Microw. Theory Techn.*, vol. 68, no. 11, pp. 4652–4661, Nov. 2020.

[15] J. Schorlemer, C. Schulz, N. Pohl, I. Rolfes, and J. Barowski, "Compensation of sensor movements in short-range FMCW synthetic aperture radar algorithms," *IEEE Trans. Microw. Theory Techn.*, vol. 69, no. 11, pp. 5145–5159, Nov. 2021.

[16] S. M. M. Islam, L. C. Lubecke, C. Grado, and V. M. Lubecke, "An adaptive filter technique for platform motion compensation in unmanned aerial vehicle based remote life sensing radar," in *Proc. 50th Eur. Microw. Conf. (EuMC)*, Jan. 2021, pp. 937–940.

[17] T. M. Seppänen, J. Kananen, K. Noponen, O.-P. Alho, and T. Seppänen, "Accurate measurement of respiratory airflow waveforms using depth data," in *Proc. 37th Annu. Int. Conf. IEEE Eng. Med. Biol. Soc. (EMBC)*, Aug. 2015, pp. 7857–7860.

[18] S. M. M. Islam, O. Boric-Lubecke, and V. M. Lubecke, "Identity authentication in two-subject environments using microwave Doppler radar and machine learning classifiers," *IEEE Trans. Microw. Theory Techn.*, vol. 70, no. 11, pp. 5063–5076, Nov. 2022.

[19] B.-K. Park, O. Boric-Lubecke, and V. M. Lubecke, "Arctangent demodulation with DC offset compensation in quadrature Doppler radar receiver systems," *IEEE Trans. Microw. Theory Techn.*, vol. 55, no. 5, pp. 1073–1079, May 2007.

[20] RFbeam Microwave GmbH.(2024). *K-MC1 24 GHz Doppler Radar Module: Datasheet and Application Notes*. Accessed: Dec. 3, 2024. [Online]. Available: https://www.rfbeam.ch

[21] F. Tian et al., "An FFT-based DC offset compensation and I/Q imbalance correction algorithm for bioradar sensors," *IEEE Trans. Microw. Theory Techn.*, vol. 72, no. 3, pp. 1900–1910, Mar. 2024.

[22] Z. Chen, W. Xu, S. Dong, R. Ma, C. Gu, and X. Zhang, "Radar sensing of displacement motions with high robustness against additive noise," *IEEE Trans. Microw. Theory Techn.*, vol. 71, no. 8, pp. 3678–3690, Aug. 2023.

[23] A. Singh et al., "Data-based quadrature imbalance compensation for a CW Doppler radar system," *IEEE Trans. Microw. Theory Techn.*, vol. 61, no. 4, pp. 1718–1724, Apr. 2013.

[24] W. Li, Y. Xiong, C. Wei, S. Chen, W. Fan, and Z. Peng, "A robust and widely applicable compensation method for quadrature imbalance of Doppler radar," *IEEE Trans. Microw. Theory Techn.*, vol. 72, no. 11, pp. 6507–6517, Nov. 2024, doi: 10.1109/TMTT.2024.3402583.

[25] S. Rogers, "Adaptive filter theory," *Control Eng. Pract.*, vol. 4, no. 11, pp. 1629–1630, 1996.

[26] M. H. Hayes, *Statistical Digital Signal Processing and Modeling*. Hoboken, NJ, USA: Wiley, 1996.

[27] A. D. Droitcour, O. Boric-Lubecke, V. M. Lubecke, J. Lin, and G. T. A. Kovacs, "Range correlation and I/Q performance benefits in single-chip silicon Doppler radars for noncontact cardiopulmonary monitoring," *IEEE Trans. Microw. Theory Techn.*, vol. 52, no. 3, pp. 838–848, Mar. 2004.

[28] A. Nayyar and V. Puri, "A review of beaglebone smart board's—A linux/Android powered low cost development platform based on ARM technology," in *Proc. 9th Int. Conf. Future Gener. Commun. Netw. (FGCN)*, Nov. 2015, pp. 55–63.

Khaldoon M. Ishmael (Member, IEEE) received the ASNS degree in engineering from Leeward Community College, Pearl City, HI, USA, in 2015, and the B.S., M.S., and Ph.D. degrees in electrical engineering from the University of Hawai'i at Mānoa, Honolulu, HI, USA, in 2017, 2018, and 2023, respectively.

In the summer of 2015 and 2016, he was selected for the DoD Pathways Internship Program. In the summer of 2017 and 2018, through the Naval Research Enterprise Internship Program. He was an Engineering Research Intern with the Naval Information Warfare Center Pacific, Pearl City, where his research focused on wafer-scale integration technologies for wireless and optical communications. His research on RF microwave sensor interests includes noninvasive physiological sensors, radar systems, antenna array signal processing, adaptive filter techniques, and radar subject separation methods.

Dr. Ishmael was a recipient of the four-year Department of Defense (DoD) Science, Mathematics, and Research for Transformation (SMART) Scholarship in 2019, the 2021 Frederick M. Kresser Advancing Science in America (ARCS) Award in Engineering at the University of Hawai'i, the Nationwide DoD Smart Scholar and Mentor Award for Studying Doppler Radar Physiological Sensing, and the Outstanding Ph.D. Student Award in 2023.

Shekh M. M. Islam (Senior Member, IEEE) received the B.Sc. and M.Sc. degrees (Hons.) in electrical and electronic engineering from the University of Dhaka, Dhaka, Bangladesh, in 2012 and 2014, respectively, and the Ph.D. degree in electrical engineering from the University of Hawai'i at Mānoa, Honolulu, HI, USA, in December 2020, focusing on biomedical applications incorporating RF/Microwave technologies.

He has been an Assistant Professor with the Department of Electrical and Electronic Engineering, University of Dhaka, since 2022. He worked as a JSPS Invitational Fellow at Kyoto University, Kyoto, Japan. From 2014 to 2016, he was a Lecturer with the Department of Electrical and Electronic Engineering, University of Dhaka. In the summer of 2019, he worked as a Radar Systems and Applications Engineering Intern with ON Semiconductor, Phoenix, AZ, USA. His research interests include radar systems, antenna array signal processing, adaptive filter techniques, and machine-learning classifiers for pattern recognition.

Dr. Islam has been an Affiliate of the Technical Committee of the MTT-28 Biological Effects and Medical Applications of the IEEE Microwave Theory and Techniques Society. He was a recipient of the 2020 University of Hawaii at Manoa Department of Electrical Engineering Research Excellence Award. He was the Student Paper Finalist at the IEEE Radio Wireless Week (RWW'19) Conference in FL, USA. He served as an Editorial Board Member of the Frontiers in Physiology Journal and as a Review Editor of IEEE ACCESS, IEEE SENSORS, IEEE TRANSACTIONS ON MICROWAVE THEORY AND TECHNIQUES, *MDPI Sensors*, *Frontiers in Sensors*, and *Frontiers in Communication and Network Journals*.

Mohammad Shadman Ishrak (Graduate Student Member, IEEE) received the B.Sc. and M.Sc. degrees from the University of Dhaka, Dhaka, Bangladesh, in 2018 and 2020, respectively. He is currently pursuing the Ph.D. degree with the Department of ECE, University of Hawai'i at Mānoa, Honolulu, HI, USA.

His current work involves the analysis of demodulation techniques and their efficiency in interpreting Doppler radar signals for applications. His research interests lie in noninvasive vital sign detection, cardiopulmonary signal processing, identity authentication, and posture classification through RF sensors.

Jannatun Noor Sameera (Graduate Student Member, IEEE) received the B.S. and M.S. degrees in electrical and electronic engineering from the University of Dhaka, Dhaka, Bangladesh, in 2018 and 2020, respectively. She is currently pursuing the Ph.D. degree in electrical and computer engineering with the University of Hawai'i at Mānoa, Honolulu, HI, USA.

Her research interests include RF and microwave, circuit design, physiological signal processing, physiological monitoring sensors, noncontact vital signs data acquisition, and wireless health monitoring systems.

Richard C. Ordoñez (Member, IEEE) was born in Plattsburgh, NY, USA, in 1986. He received the B.S. degree in electrical engineering and the Ph.D. degree in electrophysics from the University of Hawai'i at Mānoa, Honolulu, HI, USA, in 2009 and 2016, respectively.

His dissertation proved the functionality of flexible graphene devices fabricated with novel materials such as liquid metal and honey. He joined the Advanced Development and Experimentation Branch at the Naval Information Warfare Center, Pearl City, HI, USA, in 2016, where he currently serves as a Scientist/Electronics Engineer. He currently has 18 publications and holds five issued patents. His research interests include nanoparticles, two-dimensional-based electronic devices, photonics, adaptive optics, flexible electronics, and unmanned systems.

Dr. Ordoñez was a recipient of the Department of Navy Pathways Internship and Achievement Reward for the College Scientists Foundation Award in 2014. He was Inducted as the youngest Distinguished Member of the National Academy of Inventors, Hawaii Chapter 2015, for Graphene-Based Technologies Using Liquid Metal Electrodes. He received the Navy's Top Emergent Investigator Award from the Pentagon in 2017 and was recognized with the DoD SMART Scholarship Scholar and Mentor of the Year Award in 2021 and the Navy Civilian Service Commendation Medal in 2023.

Victor M. Lubecke (Fellow, IEEE) received the B.S. degree in electrical and electronics engineering from California State Polytechnic University, Pomona, CA, USA, in 1986, and the M.S. and Ph.D. degrees in electrical engineering from California Institute of Technology, Pasadena, CA, in 1990 and 1995, respectively.

He is an Electrical and Computer Engineering Professor at the University of Hawai'i at Mānoa, Honolulu, HI, USA. He was previously with Bell Laboratories, Lucent Technologies, Murray Hill, NJ, USA, where his research focused on remote sensing technologies for biomedical and industrial applications and microelectromechanical systems (MEMS) and 3-D wafer-scale integration technologies for wireless and optical communications. Before that, he worked for NASA Jet Propulsion Laboratory (JPL), Pasadena, CA, USA, and the Institute for Physical and Chemical Research (RIKEN), Sendai, Japan, where his research involved terahertz and MEMS receiver technologies for space remote sensing and communications applications. He was the Co-Founder and the CTO of Kai Medical, Inc., Honolulu, and the Co-Founder of Adnoviv Inc., Honolulu, HI, USA, where he is the Vice President. He has authored or co-authored more than 250 peer-reviewed research articles and holds eight U.S. patents. His research interests include remote sensing, biomedical sensors, MEMS, heterogeneous integration, and microwave/terahertz radio.

Prof. Lubecke was a member of the MTT Technical Committees for Terahertz Technology and Applications and Biological Effects and Medical Applications. He is a Fulbright Scholar, an Emeritus Distinguished Microwave Lecturer of the IEEE Microwave Theory and Techniques (MTT) Society, and a Speakers Bureau Speaker. He served as the Vice-Chair for the IEEE International Microwave Symposium (IMS) in 2017. He served as a Topic Editor for IEEE TRANSACTIONS ON TERAHERTZ SCIENCE AND TECHNOLOGY.

Olga Borić-Lubecke (Fellow, IEEE) received the B.Sc. degree in electrical engineering from the University of Belgrade, Belgrade, Serbia, in 1989, the M.S. degree in electrical engineering from California Institute of Technology, Pasadena, CA, USA, in 1990, and the Ph.D. degree in electrical engineering from the University of California at Los Angeles, Los Angeles, CA, in 1995.

She is an Electrical and Computer Engineering Professor at the University of Hawai'i at Mānoa (UH), Honolulu, HI, USA. Before joining UH, she was with Bell Laboratories and Lucent Technologies, Murray Hill, NJ, USA; the Institute of Physical and Chemical Research (RIKEN), Sendai, Japan; and the NASA Jet Propulsion Laboratory, Pasadena, CA, USA, where she conducted research in RFIC technology and biomedical applications of wireless systems. She is the Co-Founder and the Chief Technical Advisor of a Start-Up Company, Kai Medical, Honolulu, and the Co-Founder and the President of Adnoviv Inc., Honolulu. She has authored over 250 journal and conference publications, two books, and several book chapters. She holds three patents, and various media outlets have featured her research. Her research interests include wireless circuits and systems, biomedical applications, and renewable energy.

Prof. Borić-Lubecke is a Fulbright Scholar, a Foreign Member of the Academy of Engineering of Serbia, and a Distinguished Member of the National Academy of Inventors, UH Chapter. She was a co-recipient of the Emerging Technology Award from TechConnect 2007. She was the Adviser-Author of several award-winning IEEE Microwave Theory and Techniques Society Student Papers and IEEE Engineering in Medicine and Biology Society Student Papers. She was the Workshop Chair for the 2003 IEEE IMS, the Technical Program Vice-Chair for the 2007 IEEE IMS, the Technical Program Co-Chair for the 2017 IEEE IMS, and the 2018 IEEE IMS Technical Program Advisor. She was an Associate Editor of IEEE MICROWAVE AND WIRELESS COMPONENTS LETTERS and IEEE TRANSACTIONS ON MICROWAVE THEORY AND TECHNIQUES.